A Novel Biphase Complementary Code Sidelobe Suppression Method

Liyu Tian,Yiding Liang, Miao He, Baopeng Sun

Abstract—**The effectiveness of sidelobe suppression in complementary code radar signals is significantly compromised by phase distortions arising from Doppler shifts. This study proposes a novel bi-phase complementary code sidelobe suppression technique, termed Enhanced Broad Doppler Tolerance (EBDT), designed to improve resilience to Doppler effects. The method employs the Moving Target Detection (MTD) algorithm to estimate Doppler frequency and subsequently segments the complementary signal into two distinct data matrices. Through rigorous analytical derivation, a phase compensation factor is developed to counteract Doppler-induced phase distortions, thereby restoring the sidelobe cancellation properties of the autocorrelation function. Simulation results demonstrate that, compared to existing approaches, the EBDT method achieves superior Doppler tolerance, reduced mainlobe attenuation, and an enhanced signal-to-noise ratio.**

Index Terms—**Biphase complementary code, Sidelobe suppression, Doppler compensation, Moving Target Detection**

I. INTRODUCTION

Contemporary warfare demands radar systems capable of both detecting hostile targets and evading electronic reconnaissance to mitigate the threat of anti-radiation missile strikes, thereby enhancing battlefield survivability. Phase-coded signals with large time-bandwidth products offer superior low probability of intercept (LPI) performance. However, these signals exhibit two significant limitations: (1) limited Doppler tolerance [1], [2], [3], leading to substantial signal energy loss during pulse compression for high-velocity targets; and (2) elevated range sidelobes following pulse compression [4], [5], [6], where the sidelobes of a larger target may mask the mainlobe of a smaller target, thereby impairing the radar's ability to detect the latter.

Manuscript received May 16, 2025; revised July 9, 2025.

Liyu Tian is an associate professor of the School of Integrated Circuits and Electronics, Beijing Institute of Technology, Beijing, 100081 China (corresponding author to provide phone: +86-010-68912614; e-mail: tianliyu@bit.edu.cn).

Yiding Liang is a postgraduate student of the School of Integrated Circuits and Electronics, Beijing Institute of Technology, Beijing, 100081 China (e-mail: liang_yd2021@163.com).

Miao He is a Master's student of the School of Integrated Circuits and Electronics, Beijing Institute of Technology, Beijing, 100081 China (e-mail: hemiao@oppo.com).

Baopeng Sun is a Master's student of the School of Integrated Circuits and Electronics, Beijing Institute of Technology, Beijing, 100081 China (e-mail: yongshikobe@126.com).

Complementary code signals offer a theoretical solution to the sidelobe challenges inherent in phase-coded signals [7]. When implemented in radar pulse waveforms, complementary code pairs provide two primary benefits: (a) pulse compression to the duration of a single code element, and (b) complete suppression of sidelobes in the autocorrelation function (ACF) across the entire pulse duration [8]. However, despite their ability to eliminate sidelobes under ideal conditions, complementary codes demonstrate similarly limited Doppler tolerance [9], [10], compromising their performance in dynamic environments.

Reference [11] introduced a method for optimizing transmission sequences using first-order Reed-Muller (RM) codes, which systematically generates complementary waveform sequences to significantly enhance waveform resilience in specific Doppler environments. Similarly, Calderbank and Pezeshki [12], [13] utilized Prouhet–Thue–Morse (PTM) sequences to optimize the transmission order of Golay complementary waveforms, effectively suppressing range sidelobes in zero-Doppler narrowband conditions. The binomial design (BD) approach, developed by Dang [14], [15], extends the sidelobe suppression region by optimizing matched filter weights; however, it struggles to maintain adequate Doppler resilience for high-velocity targets. References [16] and [17] independently proposed the point-wise minimization processor (PMP) and point-wise threshold processor (PTP) techniques, which effectively combine the strengths of RM and BD methods to enhance Doppler resolution and optimize sidelobe suppression, achieving robust narrowband Doppler tolerance. Additionally, Reference [18] presented an optimization approach based on high-order null constraints, constructing adaptable sidelobe suppression regions by solving suboptimization problems. This method maintains excellent sidelobe suppression performance even under significant Doppler shifts, although it requires prior knowledge of the target's motion velocity.

To address the identified challenges, this study introduces a novel methodology for sidelobe suppression within complementary signal ranges, characterized by its Enhanced Broad Doppler Tolerance (EBDT). The proposed approach begins with the segmentation of complementary signals into two distinct data matrices. The Moving Target Detection (MTD) algorithm is utilized to estimate Doppler frequencies, enabling the effective classification of targets with varying velocities into corresponding Doppler bins. By analyzing phase disparities induced by Doppler shifts across the elements of the data matrices, phase compensation factors are analytically derived. These factors are subsequently applied to the respective matrix elements to counteract the modulatory

effects of Doppler frequencies on the complementary signals, thereby restoring the robust sidelobe cancellation properties of their autocorrelation functions. Following this, pulse compression is executed along the range dimension for both data matrices, succeeded by coherent summation of the complementary sequences to eliminate sidelobes. The implementation of this methodology yields a low peak sidelobe ratio (PSLR), demonstrating substantial enhancements in sidelobe suppression and resilience to Doppler effects.

II. Complementary Signal Processing Method

A. Signal Model

Let $X_A=[a_0,...,a_{P-1}]$ and $X_B=[b_0,...,b_{P-1}]$ represent binary sequences of length P, where $a_n,b_n\in\{-1,1\}$ for $n=0,...,P-1$. These sequences are designated as a complementary pair if their autocorrelation functions (ACF) satisfy the condition:

$$R_A[k]+R_B[k]=2P\delta[k] \tag{1}$$

Where $R_A[k]$ and $R_B[k]$ respectively denotes the autocorrelation function of X_A and X_B at lag k, and $\delta[k]$ represents the Kronecker delta function.

Consider the biphase-coded signals $x_A(t)$ and $x_B(t)$, which are modulated by the complementary sequence pair X_A and X_B :

$$x_A(t)=\sum_{n=0}^{P-1}a_n c(t-nt_c) \tag{2}$$

$$x_B(t)=\sum_{n=0}^{P-1}b_n c(t-nt_c) \tag{3}$$

Where $c(t)$ denotes a unit-energy baseband pulse signal with pulse width t_c .

In a coherent processing time (CPI) containing M pulse repetition intervals (PRI), the transmission order of the complementary signals $x_A(t)$ and $x_A(t)$ is governed by the sequence $S=[s_0,...,s_{M-1}]$, where $s_m\in\{0,1\}$, $\overline{s}_m=1-s_m$ for $m=0,...,M-1$. The the corresponding baseband signals is:

$$u_s(t)=\sum_{m=0}^{M-1}s_m x_A(t-mT)+\overline{s}_m x_B(t-mT) \tag{4}$$

Weight the transmitted signal $u_s(t)$ with the weight vector $W=[w_0,...,w_{M-1}]$, where $w_m>0$, $m=0,...,W-1$.

$$u_w(t)=\sum_{m=0}^{M-1}w_m\left\{s_m x_A(t-mT)+\overline{s}_m x_B(t-mT)\right\} \tag{5}$$

The impulse response function of the receiving filter is denoted as $u_w^*(-t)$. The cross ambiguity function (CAF) of the signals $u_s(t)$ and $u_w(t)$, which represents the time-domain response of the filter to the input signal $u_s(t)e^{j\omega t}$, is defined as follows:

$$\chi_{s,w}(\tau,\omega)=\int_{-\infty}^{+\infty}u_s(t)u_w^*(t-\tau)e^{j\omega t}dt \tag{6}$$

The continuous-time delay is discretized with an interval t_c , and assuming the intrapulse Doppler shift is negligible, the discrete-time cross-ambiguity function (CAF) can be expressed as:

$$\begin{aligned}R_{S,W}(k,\theta)&=\sum_{m=0}^{M-1}w_m R_{X(m)}[k]e^{j\theta m}\\&=\frac{1}{2}(R_A[k]+R_B[k])\sum_{m=0}^{M-1}w_m e^{j\theta m}+\\&\quad\frac{1}{2}(R_A[k]-R_B[k])\sum_{m=0}^{M-1}(-1)^{s_m}w_m e^{j\theta m}\end{aligned} \tag{7}$$

Where $\theta=\omega T$, ω denotes the Doppler angular frequency. According to (1), the first term in (7) vanishes at $k\neq 0$, indicating that its contribution is confined to the mainlobe region [18]. In contrast, the formation of the sidelobes is governed by the second term, which dictates their amplitude and distribution. Let:

$$f(\theta)=\sum_{m=0}^{M-1}(-1)^{s_m}w_m e^{j\theta m} \tag{8}$$

The objective of sidelobe suppression is redefined as minimizing the function $f(\theta)$ to approach zero. According to reference [19], this is accomplished by introducing high-order nulls in $f(\theta)$ at a designated θ through the strategic selection of parameters **S** and **W**. Nevertheless, this technique necessitates prior knowledge of the target's velocity, and the choice of **W** critically affects the output SNR of the receiving filter. This study employs a matched filter approach, setting $\mathbf{W}=\alpha\mathbf{1}$, to optimize the SNR. To satisfy the condition $f(\theta)=0$, the following criteria are essential:

1) Let **S** be an alternating sequence of 0 and 1;
2) Achieve $\theta=0$ through phase compensation.

B. Algorithm Development

The model for signal transmission and reception within the radar system is depicted in Fig. 1. At the transmitter, complementary baseband signals are modulated and transmitted in an alternating manner. At the receiver, a quadrature receiver is employed to demodulate the incoming radio frequency signals. The resuling complex baseband signals are then stored in the data matrix **E**.

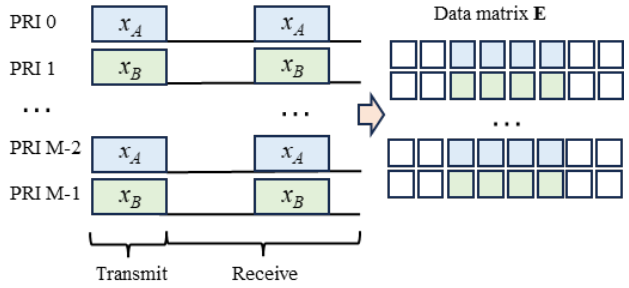

Fig. 1 Complementary signal transmission and reception model

The data matrix **E** is split into two submatrices, $\mathbf{A}^1$ and $\mathbf{B}^1$, based on odd and even rows.

$$A^1=\begin{bmatrix} e_{00} & e_{01} & \cdots & e_{0(n-1)} \\ e_{20} & e_{21} & \cdots & e_{2(n-1)} \\ \cdots & \cdots & e_{kl} & \cdots \\ e_{(M-2)0} & e_{(M-2)1} & \cdots & e_{(M-2)(n-1)} \end{bmatrix} \tag{9}$$

$$B^1=\begin{bmatrix} e_{10} & e_{11} & \cdots & e_{1(n-1)} \\ e_{30} & e_{31} & \cdots & e_{3(n-1)} \\ \cdots & \cdots & e_{(k+1)l} & \cdots \\ e_{(M-1)0} & e_{(M-1)1} & \cdots & e_{(M-1)(n-1)} \end{bmatrix} \tag{10}$$

Doppler compensation is achieved through the application of phase compensation factors, as detailed in [20]. The derivation of the phase compensation factor is presented as follows:

The Doppler frequency introduces a phase difference of $2\pi f_d/f_s$ between adjacent elements in the same row of matrices $\mathbf{A}^1$ and $\mathbf{B}^1$, and a phase difference of $4\pi f_d/f_s$ between adjacent elements in the same column. The phase relationship between element e_{00} and element e_{kl} is as follows:

$$e_{kl}=s_{kl}e_{00}\exp[j2\pi f_d(\frac{2k}{f_x}+\frac{l}{f_s})] \tag{11}$$

where s_{kl} takes the value of -1 or 1, determined by a binary pseudorandom sequence representing the ratio of the symbol values (-1, +1) corresponding to e_{00} and e_{kl}. Without considering range migration, the symbol of the elements in the same column of the data matrix are identical. Perform FFT on each column of matrix $\mathbf{A}^1$ to obtain matrix $\tilde{\mathbf{A}}$. The l-th column elements of matrix $\tilde{\mathbf{A}}$ are denoted as $\tilde{\mathbf{A}}_l(h)$, where $h=[0,1,...,M/2-1]$.

$$\begin{aligned}\tilde{\mathbf{A}}_l(h)&=\sum_{k=0}^{M/2-1}e_{(2k)l}\exp(\frac{-j2\pi hk}{M/2})\\&=\sum_{k=0}^{M/2-1}s_{(2k)l}e_{00}\exp[j2\pi f_d(\frac{4k}{f_x}+\frac{l}{f_s})]\exp(\frac{-j2\pi hk}{M/2})\\&=s_{0l}\sum_{k=0}^{M/2-1}e_{00}\exp[j2\pi f_d(\frac{4k}{f_x}+\frac{l}{f_s})]\exp(\frac{-j2\pi hk}{M/2})\\&=s_{0l}e_{00}\exp(j2\pi\frac{f_dl}{f_s})\sum_{k=0}^{M/2-1}\exp[j2\pi k(\frac{2f_d}{f_x}-\frac{2h}{M})]\\&=\begin{cases}0 & h\neq\dfrac{Mf_d}{f_x}\\ \dfrac{s_{0l}e_{00}M}{2}\exp(j2\pi\dfrac{f_dl}{f_s}) & h=\dfrac{Mf_d}{f_x}\end{cases}\end{aligned} \tag{12}$$

The compensation factor $p_{A,hl}$ for $\tilde{\mathbf{A}}_l(h)$ is:

$$p_{A,kl}=\exp(-j2\pi\frac{f_dl}{f_s})=\exp(-j2\pi\frac{hlf_x}{Mf_s}) \tag{13}$$

Perform FFT on each column of matrix $\mathbf{B}^1$ to obtain matrix $\tilde{\mathbf{B}}$. Based on the above derivation process, it can be concluded that:

$$\tilde{\mathbf{B}}_l(h)=\begin{cases}0 & h\neq\dfrac{Mf_d}{f_x}\\ \dfrac{s_{0l}a_{10}M}{2}\exp(j2\pi\dfrac{f_dl}{f_s}) & h=\dfrac{Mf_d}{f_x}\end{cases} \tag{14}$$

Since there is also a phase difference $\exp[j2\pi f_d/f_x]$ between e_{10} and e_{00} caused by Doppler frequency, the compensation factor $p_{B,hl}$ for $\tilde{\mathbf{B}}_l(h)$ is:

$$\begin{aligned}p_{B,hl}&=\exp(-j2\pi\frac{f_dl}{f_s})\exp(-j2\pi\frac{f_d}{f_x})\\&=\exp(-j2\pi\frac{hf_x}{M}[\frac{l}{f_s}+\frac{1}{f_x}])\end{aligned} \tag{15}$$

The progression of the algorithm is depicted in Fig. 2. Following phase compensation of the signals, pulse compression is performed on matrices $\tilde{\mathbf{A}}$ and $\tilde{\mathbf{B}}$ along the range dimension. This process yields the compressed matrices $\mathbf{A}^2$ and $\mathbf{B}^2$. Subsequently, the corresponding rows of matrices $\mathbf{A}^2$ and $\mathbf{B}^2$ are summed to achieve the superposition of complementary code autocorrelation functions, thereby effectively reducing the range sidelobes.

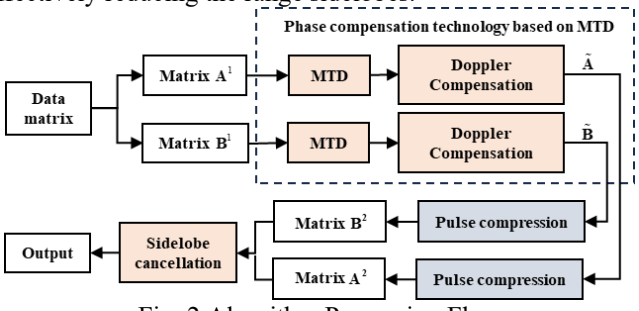

Fig. 2 Algorithm Processing Flow

C. Performance Metrics

Four common metrics in the field of sidelobe suppression are employd to evaluate algorithm performance.

a. Normalized signal-to-noise ratio

In the presence of additive white Gaussian noise with power N_0 at the filter input, the noise power N at the filter output is given by:

$$N=N_0\int_{-\infty}^{\infty}|u_w(t)|^2\,dt=N_0M\|\mathbf{w}\|_2^2 \tag{16}$$

The SNR at the filter output is:

$$\mathrm{SNR}=10\lg\frac{\sigma^2|R_{s,w}(0,0)|^2}{N}=10\lg\tilde{\sigma}\frac{\|\mathbf{w}\|_1^2}{\|\mathbf{w}\|_2^2} \tag{17}$$

Where $\tilde{\sigma}=\dfrac{P\sigma^2}{N_0}$ is independent of the filter parameters. The normalized signal-to-noise ratio (NSNR) is defined as:

$$\mathrm{NSNR}=10\lg\frac{\|\mathbf{w}\|_1^2}{M\|\mathbf{w}\|_2^2} \tag{18}$$

b. Peak sidelobe ratio

The peak sidelobe ratio (PSLR) is defined as the ratio between the maximum range sidelobe and the mainlobe, expressed in decibels as.

$$\eta(\theta)=20\lg\left(\frac{\max\limits_{k\neq 0}\left|R_{s,w}(k,\theta)\right|}{\left|R_{s,w}(0,\theta)\right|}\right),\theta\in[0,\pi] \tag{19}$$

c. Mainlobe Attenuation

Mainlobe attenuation quantifies the degree of reduction in the mainlobe amplitude under Doppler frequency shift conditions relative to its maximum value, given by:

$$L(\theta)=20\lg\frac{\left|R_{s,w}(0,\theta)\right|}{\left|R_{s,w}(0,0)\right|},\theta\in[0,\pi] \tag{20}$$

d. Doppler Tolerance

Doppler tolerance is defined as the operational range within which a radar system maintains effective functionality despite the presence of Doppler frequency shifts. In the context of this study, it is specifically delineated as the region where the peak sidelobe ratio remains below -50 dB.

$$\left\{\theta\in[0,\pi]\middle|\eta(\theta)\le -50dB\right\} \tag{21}$$

III. Experimental Results and Analysis

Consider complementary code sequences with a code length of 512 and a code width of 0.2 us. The number of coherently integrated pulses (CIP) is 256, consisting of 128 pairs of complementary signals. The PRI is set at 300 μs, and the carrier frequency is 1 GHz. The baseband echo signal is obtained through digital down conversion. Subsequently, the baseband signal undergoes processing techniques, including MTD, phase compensation, and pulse compression, culminating in an assessment of the sidelobe suppression performance.

A. Ablation Analysis

When the target Doppler frequency aligns exactly with an FFT Doppler bin, the sidelobe cancellation without phase compensation achieves a PSLR of –29.83 dB, as shown in Fig. 3(a). After applying phase compensation, the PSLR improves dramatically to approximately –160 dB, as depicted in Fig. 3(b) representing an enhancement of over 130 dB in sidelobe suppression. This demonstrates the substantial benefit of the proposed method in ideal alignment conditions.

To assess performance under frequency misalignment, PSLR values were measured for targets located at fractional Doppler bin positions ranging from 0.1 to 0.9 bin offsets. Results indicate that straddle loss increases with fractional-bin displacement, peaking at the midpoint (0.5 bin offset) between two adjacent Doppler bins. At this worst-case offset (bin No.25.5), the PSLR without compensation is –29.64 dB, as shown in Fig. 4(a), while with phase compensation it improves to –64.10 dB, as illustrated in Fig. 4(b), representing a suppression gain of 34.46 dB.

As shown in Fig. 5(a), when dealing with multi-target echo signals, a significant difference in radar cross-section (RCS) between targets (5:500:1) can hinder detection. Without phase compensation, smaller targets may be obscured by the range sidelobes of the larger target, rendering them undetectable. However, after the implementation of phase compensation, the sidelobes of the three targets are significantly suppressed, as shown in Fig. 5(b). This enhancement facilitates the detection of smaller targets, thereby increasing the detection probability of the radar system.

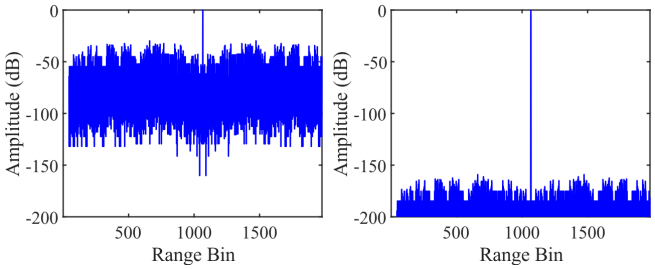

Fig. 3 Comparison of Single-target Sidelobe Cancellation Performance on Doppler bin No.25: (a) Without Phase Compensation (b) With Phase Compensation

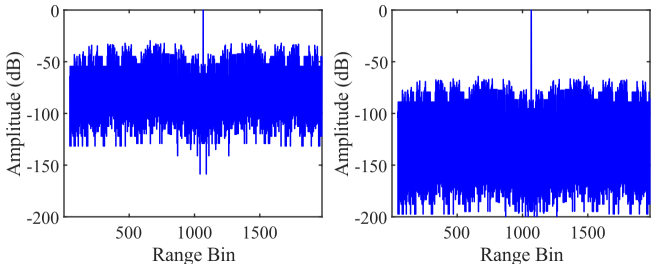

Fig. 4 Comparison of Single -target Sidelobe Cancellation Performance on Doppler bin No.25.5: (a) Without Phase Compensation (b) With Phase Compensation

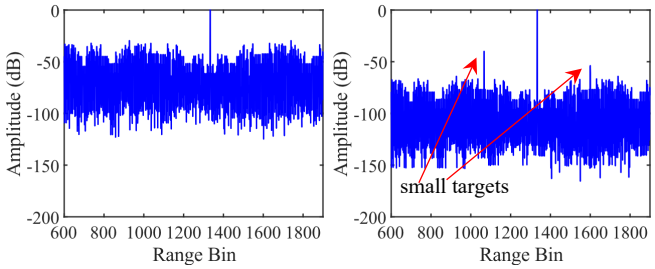

Fig. 5 Comparison of Multi-target Sidelobe Cancellation Performance on Doppler bin No.25.5: (a) Without Phase Compensation (b) With Phase Compensation

B. Algorithm Performance Evaluation

Due to the inherent quantization error of FFT-based Doppler estimation, the maximum frequency deviation can reach $\pm\Delta f_d/2$, where Δf_d denotes the Doppler bin width. This estimation uncertainty induces a residual phase error $\hat{\theta}\in[-\pi/M,\pi/M]$ after phase compensation, where M denotes the number of CIP. A scaling factor $\kappa(\hat{\theta})$ is introduced to represent the ratio of sidelobe gain to mainlobe gain under the condition where $\hat{\theta}\neq 0$.

$$\kappa(\hat{\theta})=\frac{\left|\sum_{m=0}^{M-1}(-1)^m e^{j\hat{\theta}m}\right|}{\left|\sum_{m=0}^{M-1}e^{j\hat{\theta}m}\right|}=\left|\frac{\sin(\frac{M(\hat{\theta}+\pi)}{2})\sin(\frac{\hat{\theta}}{2})}{\sin(\frac{\hat{\theta}+\pi}{2})\sin(\frac{M\hat{\theta}}{2})}\right| \quad (22)$$

Since M is usually a power of 2,

$$\kappa(\hat{\theta})=\left|\tan\frac{\hat{\theta}}{2}\right| \quad (23)$$

$$\eta(\hat{\theta})=20\lg(\frac{\max_{k\neq 0}\left|R_A[k]-R_B[k]\right|}{2P}\times\left|\tan\frac{\hat{\theta}}{2}\right|) \quad (24)$$

Under varying conditions of code lengths and pulse integration numbers, the maximum values of $\eta(\hat{\theta})$ resulting from the application of the algorithm are presented in TABLE 1.

TABLE 1

MAXIMUM $\eta(\hat{\theta})$ UNDER DIFFERENT CODE LENGTHS AND NUMBERS OF CIP

Code length P	Number of CIP				
	32	64	128	256	512
32	-37.20	-43.22	-49.24	-55.26	-61.28
64	-41.48	-47.50	-53.52	-59.54	-65.56
128	-41.88	-47.90	-53.92	-59.94	-65.97
256	-44.52	-50.54	-55.56	-62.58	-68.60
512	-45.25	-51.27	-57.29	-63.31	-69.33

C. Performance Comparison

Experimental conditions: The code length P is 256, the number of CIP is 128. The CAF for each method is shown in Fig. 6. The mainlobe loss and PSLR performance of methods under Doppler shift is shown in Fig. 7. The NSNR and Doppler tolerance of each method are shown in TABLE 2.

As established in the preceding analysis, the PTM, BD, and NM-DRCW methods are all derived from (8), wherein sidelobe suppression is achieved by introducing higher-order nulls. Prior work [19] has explicitly quantified the relationship between null order and the number of CIPs for the PTM and BD methods. In contrast, the NM-DRCW method offers greater flexibility in selecting the null order.

The PTM method creates a null of order $Z=\log_2 128-1=6$ at $\theta=0$. Due to its low order, the Doppler tolerance is narrow. As Fig. 7(a) shows, the mainlobe peak decreases rapidly as the Doppler shift increases, with the peak loss reaching 40 dB at 0.8π. This method employs a matched filter, resulting in a NSNR of 0 dB.

The BD method creats a null of order $Z=128-2=126$ at $\theta=0$, which significantly broadens Doppler tolerance compared to PTM. However, Fig. 7(b) shows that while the null depth is high, PSLR degradation is severe when Doppler exceeds 0.4π. Mainlobe loss increases at a faster rate than PTM, and NSNR is the lowest of all four methods due to binomial coefficient weighting.

The NM-DRCW method sets a null of order $Z_0=20$ at $\theta_0=0$ and a null of order $Z_0=10$ at $\theta_1=0.8\pi$. As Fig. 7(c) shows, the method can effectively suppress sidelobes at specified frequencies and its mainlobe attenuation is smoother compared to the PTM and BD methods. Due to the use of a mismatched filter, the NSNR is slightly lower than 0 dB.

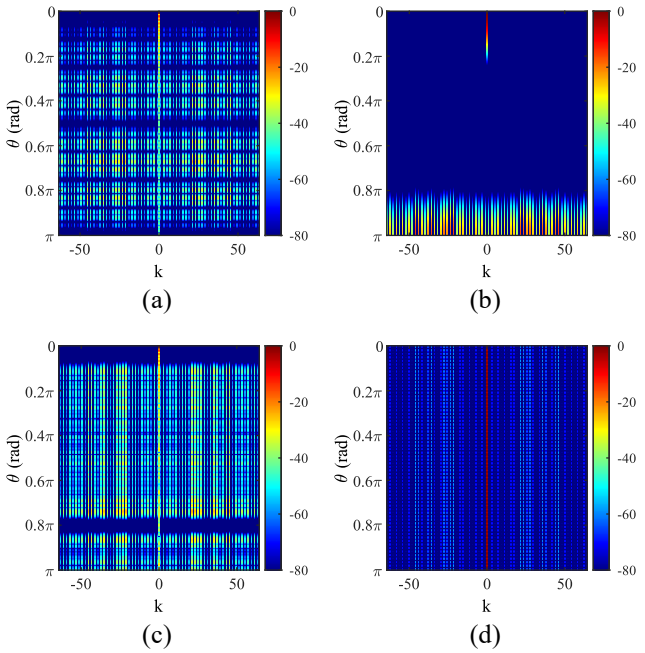

Fig. 6 Comparison of CAF for Different Methods:(a) PTM method, (b) BD method, (c) NM-DRCW method, (d) EBDT method

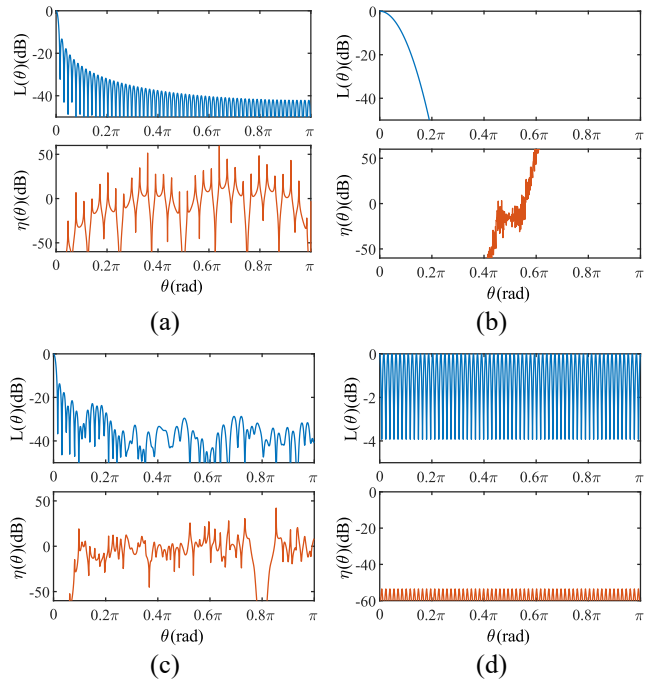

Fig. 7 Mainlobe Attenuation and PSLR Performance of Methods Under Doppler Shift: (a) PTM method, (b) BD method, (c) NM-DRCW method, (d) EBDT method

The EBDT method is suitable for scenarios where the target's velocity is unknown. As Fig. 7(d) shows, this method provides a lower sidelobe suppression level within a specific frequency range compared to the previous three methods; however, it demonstrates a substantially wider Doppler tolerance, enabling its application across a broader range of

target speeds. The proposed method induces a periodic variation in mainlobe loss as a function of Doppler shift, consistently maintaining values below 4 dB, and significantly surpasses the performance of the previous three methods. It accommodates greater Doppler mismatch, thereby preventing excessive degradation of the matched filter's output response and markedly enhancing radar detection performance [21]. Furthermore, by employing a matched filter, the method achieves a NSNR of 0 dB.

TABLE 2
THE NSNR AND DOPPLER TOLERANCE OF EACH METHOD

Method	NSNR (dB)	Doppler tolerance (rad)
PTM	0	$[0, 0.05\pi]$
BD	-8.0631	$[0, 0.41\pi]$
NM-DRCW	-0.2068	$[0, 0.07\pi] \cup [0.78\pi, 0.82\pi]$
EBDT	0	$[0, \pi]$

IV. CONCLUSION

The proposed Enhanced Broad Doppler Tolerance (EBDT) method offers an effective solution for sidelobe suppression in complementary code radar signals. The EBDT approach compensates for Doppler-induced phase distortion without requiring prior knowledge of the target's velocity, thereby reinstating the inherent sidelobe cancellation properties of complementary codes. This leads to reduced sidelobe levels and minimized mainlobe attenuation. Compared to existing technologies, EBDT enhances the NSNR through matched filter design and improves computational efficiency. Furthermore, it substantially broadens Doppler tolerance without sacrificing Doppler resolution, facilitating robust tracking and detection of multiple targets across a range of velocities.

REFERENCE

[1] M. Dikshtein, O. Longman, S. Villeval, and I. Bilik, "Automotive Radar Maximum Unambiguous Velocity Extension Via High-Order Phase Components," *IEEE Transactions on Aerospace and Electronic Systems*, vol. 58, no. 1, pp. 743–751, Feb. 2022, doi: 10.1109/TAES.2021.3103262.

[2] J. Zhu *et al.*, "Delay-Doppler Map Shaping through Oversampled Complementary Sets for High-Speed Target Detection," *Remote Sensing*, vol. 16, no. 16, p. 2898, Aug. 2024, doi: 10.3390/rs16162898.

[3] Y. Liang and L. Tian, "A Biphase Code Sidelobe Suppression Method Based on the CLEAN Algorithm," *IEEE Access*, vol. 13, pp. 105353–105360, 2025, doi: 10.1109/access.2025.3579389.

[4] P. Berestesky and E. H. Attia, "Sidelobe Leakage Reduction in Random Phase Diversity Radar Using Coherent CLEAN," *IEEE Trans. Aerosp. Electron. Syst.*, vol. 55, no. 5, pp. 2426–2435, Oct. 2019, doi: 10.1109/TAES.2018.2888652.

[5] Y. Li, W. Hu, H. Fan, and X. Du, "Phase-Coded Sequence Design for Local Shaping of Complete Second-Order Correlation," *IEEE Signal Processing Letters*, vol. 31, pp. 571–575, 2024, doi: 10.1109/LSP.2024.3359575.

[6] K. Miao, Y. Zhang, and H. Sun, "Fast Sidelobe Calculation and Suppression in Arbitrary Two-Dimensional Phased Arrays," *IEEE Antennas Wirel. Propag. Lett.*, vol. 20, no. 6, pp. 928–932, Jun. 2021, doi: 10.1109/LAWP.2021.3067380.

[7] E. Kalashnikov, "An Introduction to Golay Complementary Sequences," *Eureka*, vol. 4, no. 1, pp. 40–48, Jul. 2014, doi: 10.29173/eureka22829.

[8] N. Levanon and I. Cohen, "Performance Difference Between Differently-Coded, Same-Length, Binary Complementary Pairs," in *2022 IEEE Radar Conference (RadarConf22)*, Mar. 2022, pp. 1–5. doi: 10.1109/RadarConf2248738.2022.9764311.

[9] Y. Dong, "Implementable phase-coded radar waveforms featuring extra-low range sidelobes and Doppler resilience," *IET Radar Sonar & Navi*, vol. 13, no. 9, pp. 1530–1539, Sep. 2019, doi: 10.1049/iet-rsn.2018.5631.

[10] S. Hong, F. Zhou, Y. Dong, Z. Zhao, Y. Wang, and M. Yan, "Chaotic Phase-Coded Waveforms With Space-Time Complementary Coding for MIMO Radar Applications," *IEEE Access*, vol. 6, pp. 42066–42083, 2018, doi: 10.1109/ACCESS.2018.2859404.

[11] S. Suvorova, S. Howard, B. Moran, R. Calderbank, and A. Pezeshki, "Doppler Resilience, Reed-Müller Codes and Complementary waveforms," in *2007 Conference Record of the Forty-First Asilomar Conference on Signals, Systems and Computers*, Nov. 2007, pp. 1839–1843. doi: 10.1109/ACSSC.2007.4487553.

[12] R. Calderbank, S. D. Howard, and B. Moran, "Waveform Diversity in Radar Signal Processing," *IEEE Signal Processing Magazine*, vol. 26, no. 1, pp. 32–41, Jan. 2009, doi: 10.1109/MSP.2008.930414.

[13] A. Pezeshki, A. R. Calderbank, W. Moran, and S. D. Howard, "Doppler Resilient Golay Complementary Waveforms," *IEEE Trans. Inform. Theory*, vol. 54, no. 9, pp. 4254–4266, Sep. 2008, doi: 10.1109/TIT.2008.928292.

[14] W. Dang, A. Pezeshki, S. Howard, W. Moran, and R. Calderbank, "Coordinating complementary waveforms for sidelobe suppression," in *2011 Conference Record of the Forty Fifth Asilomar Conference on Signals, Systems and Computers (ASILOMAR)*, Pacific Grove, CA, USA: IEEE, Nov. 2011, pp. 2096–2100. doi: 10.1109/ACSSC.2011.6190398.

[15] W. Dang, A. Pezeshki, S. D. Howard, W. Moran, and R. Calderbank, "Coordinating Complementary Waveforms for Suppressing Range Sidelobes in a Doppler Band," Jan. 26, 2020, *arXiv*: arXiv:2001.09397. doi: 10.48550/arXiv.2001.09397.

[16] J. Zhu, Y. Song, C. Fan, and X. Huang, "Nonlinear processing for enhanced delay-Doppler resolution of multiple targets based on an improved radar waveform," *Signal Processing*, vol. 130, pp. 355–364, Jan. 2017, doi: 10.1016/j.sigpro.2016.07.025.

[17] J. Zhu, Y. Song, N. Jiang, Z. Xie, C. Fan, and X. Huang, "Enhanced Doppler Resolution and Sidelobe Suppression Performance for Golay Complementary Waveforms," *Remote Sensing*, vol. 15, no. 9, p. 2452, May 2023, doi: 10.3390/rs15092452.

[18] Z.-J. Wu, C.-X. Wang, P.-H. Jiang, and Z.-Q. Zhou, "Range-Doppler Sidelobe Suppression for Pulsed Radar Based on Golay Complementary Codes," *IEEE Signal Processing Letters*, vol. 27, pp. 1205–1209, 2020, doi: 10.1109/LSP.2020.3007093.

[19] W. Dang, A. Pezeshki, S. Howard, W. Moran, and R. Calderbank, "Coordinating complementary waveforms for sidelobe suppression," in *2011 Conference Record of the Forty Fifth Asilomar Conference on Signals, Systems and Computers (ASILOMAR)*, Pacific Grove, CA, USA: IEEE, Nov. 2011, pp. 2096–2100. doi: 10.1109/ACSSC.2011.6190398.

[20] L. Y. Tian and M. G. Gao, "A Doppler compensation method for biphase coded signals," *Journal of Beijing Institute of Technology*, vol. 22, no. 6, pp. 757–760, 2002.

[21] M. A. Richards, *Fundamentals of Radar Signal Processing, Third Edition*. New York, N.Y, 2022.